Published in final edited form as:
J Magn Reson Imaging. 2013 December ; 38(6): . doi:10.1002/jmri.24117.

Comparison of temperature processing methods for monitoring focused ultrasound ablation in the brain

Viola Rieke, Ph.D.[1], **Ron Instrella**[2], **Jarrett Rosenberg, Ph.D.**[3], **William Grissom, Ph.D.**[4], **Beat Werner, Ph.D.**[5], **Ernst Martin, Ph.D.**[5], and **Kim Butts Pauly, Ph.D.**[3]

[1]Department of Radiology and Biomedical Imaging, University of California, San Francisco, San Francisco, California [2]Department of Electrical Engineering, Stanford University, Stanford, California [3]Department of Radiology, Stanford University, Stanford, California [4]Department of Electrical Engineering, Vanderbilt University, Nashville, Tennessee [5]MR-Center, University Children's Hospital Zurich, Zurich, Switzerland

Abstract

Purpose—To investigate the performance of different reconstruction methods for monitoring temperature changes during transcranial MR-guided focused ultrasound (MRgFUS).

Materials and Methods—Four different temperature reconstruction methods were compared in volunteers (without heating) and patients undergoing transcranial MRgFUS: Single baseline subtraction, multibaseline subtraction, hybrid single baseline/referenceless reconstruction, and hybrid multibaseline/referenceless reconstruction. Absolute temperature error and temporal temperature uncertainty of the different reconstruction methods were analyzed and compared.

Results—Absolute temperature errors and temporal temperature uncertainty were highest with single baseline subtraction and lowest with hybrid multibaseline/referenceless reconstruction in all areas of the brain. Pulsation of the brain and susceptibility changes from tongue motion or swallowing caused substantial temperature errors when single or multibaseline subtraction was used, which were much reduced when the referenceless component was added to the reconstruction.

Conclusion—Hybrid multibaseline/referenceless thermometry accurately measures temperature changes in the brain with less artifacts and errors due to motion than pure baseline subtraction methods.

Keywords

MRgFUS; HIFU; transcranial; MR thermometry; motion

Introduction

Transcranial magnetic resonance-guided focused ultrasound (MRgFUS) ablation is being evaluated as a truly noninvasive tool for brain treatments (1). Focused ultrasound ablation can be used to destroy tumors or other targets in the brain with no effects onto the surrounding tissue, producing immediate and localized thermal coagulation. In addition, it can be reapplied as needed, which is different from treatments with ionizing radiation. Clinical applications for MR-guided focused ultrasound in the brain have included tumor

Corresponding author: Viola Rieke, PhD, China Basin Landing, 185 Berry Street, Suite 350, San Francisco, CA 94107. Phone: 415-353-4304, Fax: 415-353-9423, viola.rieke@ucsf.edu.

ablation (2), neuropathic pain management (3), and control of essential tremor (4), and may include the treatment of Parkinson's disease, epilepsy, vascular malformations, ischemic or hemorrhagic stroke, as well as the nonablative targeted delivery of therapeutic drugs, genes, and antibodies (5).

Using focused ultrasound therapy safely requires precise control of the ablative treatment. Before the actual treatment phase of the intervention, several low-power sonications are applied with peak temperatures of 39–42°C to confirm that the thermal spot is centered in the target location. These temperatures are known to be below the ablation threshold (3). During the treatment several high-power sonications are applied in an iterative process guided by MR thermometry. In order to induce local tissue ablation the acoustic power is stepwise increased from sonication to sonication to finally achieve a peak temperature of close to 60°C. If the brain tissue is heated to 57–60°C, protein denaturation and coagulation necrosis occurs, resulting in irreversible cell damage. While coagulation definitely occurs at 57–60°C or higher, damage can still occur at lower temperatures. Peak temperatures above 60°C are avoided to minimize risk of cavitation, hemorrhage and other morbidities. Since all injuries to the brain can have detectable functional consequences, it is extremely important to limit tissue damage to the targeted area. This requires accurate imaging techniques for localization, targeting, and real-time temperature monitoring to control the spatial extent and intensity of the deposited energy. In order to detect heating of temperatures of 39–42°C outside the target area and near bone, and to precisely measure the heating of 57–60°C to ensure coagulation but avoid cavitation, a temperature uncertainty of 1°C or lower is needed.

The role of MRI during thermal ablation is to monitor the temperature elevation and ensure that the targeted region in the brain is treated while sparing surrounding tissue. Tissue characteristics and heat conductivity are variable even among tumors of the same grading (6). Both vascular distribution and tissue perfusion rate can influence the spatial distribution of energy delivery and the volume of tissue affected by the treatment. Because of this variability, accurate temperature imaging throughout the treatment is essential for patient safety. In addition, accurate temperature estimation is necessary in all parts of the brain, not only in the region of the ablation. Some areas are prone to undesired heating: Use of a hemispherical transducer distributes the ultrasound energy over a large are of the skull. However, the base of the skull lies in the far field of the ultrasound beam, which is another area of potential heating. Therefore, temperature imaging in the brain near the skull and at the base of the skull is desired to monitor possible undesired temperature elevation in these areas.

MR thermometry based on the proton resonance frequency (PRF) shift with temperature can provide noninvasive temperature measurements (7) and is generally the method of choice in organs with sufficient water content (8). This method uses changes in the phase of gradient echo images to estimate the relative temperature change between images. For clinical MRgFUS procedures, temperature reconstruction is currently performed using baseline subtraction, where a phase image acquired before heating is subtracted from an image during heating. Baseline subtraction works well in phantoms or stationary tissues, but causes errors when motion occurs.

Several methods have been demonstrated for moving organs to overcome artifacts in the presence of repetitive or non-repetitive motion, including multibaseline subtraction (9,10), referenceless (11–13) and hybrid multibaseline/referenceless (14) thermometry. Although the brain seems to be a non-moving organs when compared to moving organs such as the liver, kidney, and heart, small motions typical in the brain affect the accuracy of temperature imaging. The presence of brain motion is known from motion sensitive sequences such as multishot diffusion-weighted imaging. In the brain, there is a combination of rigid-body

motion (including the skull motion), brain pulsation, and movement of other body parts that affect the thermometry. To minimize the skull motion the patient's head is fixated with a stereotactic frame during the procedure. Pulsatile motion in the brain is due to the expansion and contraction of the brain and intracranial vessels associated with the cardiac cycle (15) and drives cerebral spinal fluid (CSF) pulsation (16). Another source for temperature errors are susceptibility shifts caused by respiration (17), tongue or jaw movement, and swallowing.

A number of studies have demonstrated PRF-based MR thermometry in the brain, most of them in animal experiments or in volunteers without an actual temperature change or ablation. Kickhefel et al. (18) have investigated the influence of different pulse sequences and parameters on the temperature uncertainty. However, none of these studies have investigated how different temperature reconstruction methods perform. In this study, we investigate if temperature reconstruction methods developed for moving organs can decrease errors in the brain compared to single baseline subtraction. We compared a) single baseline subtraction, b) multibaseline subtraction, and c) hybrid multibaseline/referenceless thermometry on volunteer images without heating, and a) single baseline subtraction and b) hybrid multibaseline/referenceless thermometry on images from patients undergoing MRgFUS ablation in the thalamus.

Methods

PRF thermometry uses changes in the phase of gradient-echo images to estimate the relative temperature change ΔT, as given by

$$\Delta T = \frac{\Delta \phi}{\gamma \alpha B_0 TE} \quad [1]$$

where $\alpha = -0.01$ ppm/°C is the PRF change coefficient for aqueous tissue, γ is the gyromagnetic ratio, B_0 is the main magnetic field, *TE* is the echo time, and ΔΦ is the phase difference before and during heating. The method of extraction of ΔΦ from the MR images is what differentiates the different reconstruction algorithms.

Single baseline subtraction is the simplest approach and is currently used for temperature monitoring of MRgFUS applications in the brain. The complex phase difference of a baseline image, acquired before heating, and an image during heating is calculated. Several baseline images are often averaged to obtain a baseline image with improved SNR.

Multibaseline subtraction acquires a set of baseline images before heating which form a baseline library. During heating, the best baseline image or a composite image from the library is obtained based on certain criteria (9,10,14,19,20) and used for baseline subtraction.

Referenceless reconstruction estimates the heating from every individual image itself, without the use of a baseline image. The background phase inside the heating region is estimated by fitting a polynomial to the phase (11–13), which is then subtracted from the heating image. This estimation can be done with either an L2 fit (11) or an L1 fit (13).

Hybrid multibaseline/referenceless reconstruction combines referenceless and multibaseline reconstruction. The hybrid image model for image voxel *j* during treatment is given by

$$y_j = \left(\sum_{b=1}^{N_b} x_{b,j} w_b \right) e^{i(\{Ac\}_j + \theta_j)} + \varepsilon_j, \quad [2]$$

where the $\boldsymbol{x}_b$ are complex images from the baseline library, the w_b are the baseline image weights, $\boldsymbol{A}$ is a matrix of low-order polynomial functions, $\boldsymbol{c}$ is a polynomial coefficient vector, θ is the temperature-induced phase shift, and ε is Gaussian noise. The image model in Eq. (2) is fitted to the treatment image y by minimizing a penalized-likelihood cost function with respect to the multibaseline weights w, the polynomial coeffients $\boldsymbol{c}$, and the temperature-induced phase shift θ as described in detail in Grissom et al. (14)

The temperature reconstruction methods were implemented in MATLAB (Natick, MA). We used the same algorithm as described in Grissom et al. (14) for multibaseline and hybrid reconstructions. To perform a multibaseline reconstruction, the polynomial fitting was skipped. To perform the single baseline subtraction, the library size was one image and the polynomial fitting was skipped. To perform the averaged baseline subtraction, the library size was one image with the one image being a complex average of all baseline images, and the polynomial fitting was not performed.

We used the following abbreviations for the different methods: single baseline subtraction (SB), averaged baseline subtraction (AB), multi-baseline subtraction (MB), hybrid multi-baseline and referenceless reconstruction (hybrid MB+R), as well as hybrid SB+R, which perform the hybrid reconstruction but has only a single baseline image in the library.

Volunteer data

Images from three normal human volunteers were acquired at 3T (Signa HDx; GE Milwaukee, WI) using a birdcage head coil. All studies were conducted with the approval of the Institutional Review Board. The volunteers were given the instruction to remain as motionless as possible, which was facilitated by fixating the head tightly inside the coil with foam pads. Eighty consecutive sagittal brain images were acquired without heating using a spoiled gradient echo sequence with TE/TR = 12/25 ms, BW = 12.2 kHz, FOV = 28–30 cm, slice thickness 3 mm, flip angle 30°, matrix size 256 × 128, NEX = 1, acquisition time approximately 3 sec per image, resulting in a total scan time of approximately four minutes. In addition to these studies, we acquired datasets where the volunteers purposefully performed tongue or jaw movement, or took a deep breath during the MR scan.

From the 80 images acquired in each dataset, the first 30 images were used as a baseline set and the following 50 images were considered “treatment images” and reconstructed with the different methods as described above. For single baseline subtraction (SB), the last image of the baseline set was used for subtraction so that no temporal gap was present between baseline image and treatment images. For averaged baseline subtraction (AB), we combined the 30 baseline images into a single, high SNR baseline image. For multibaseline (MB) and hybrid reconstruction (hybrid MB+R), the first 30 images were used as the baseline library. We also performed hybrid with a single baseline image (hybrid SB+R), where the last image of the baseline images set was used.

We reconstructed temperature images and visually inspected the temperature artifacts apparent in the different methods. For each method, temporal temperature uncertainty maps were generated by calculating the temporal standard deviation for each pixel in the series of consecutive temperature images. Three 6×6 pixel ROIs were selected in the parietal region, the frontal region, and the cerebellum. For each ROI the absolute temperature error and spatial temperature uncertainty were calculated and compared.

Patient data

We retrospectively analyzed datasets from five patients acquired during transcranial MRgFUS. The noninvasive neurosurgical interventions were performed in a clinical 3T

MR-system (Signa HDx; GE, Milwaukee, WI) using a clinical system for transcranial MRgFUS surgery (ExAblate 4000; InSightec, Tirat Carmel, Israel) featuring a hemispheric 1024-element phased array transducer operating at 650kHz. The patients head was immobilized in an MR-compatible frame and positioned in the helmet-like cavity of the FUS transducer (Fig.1). The space between FUS transducer and head surface was filled with degassed water for ultrasound coupling and sealed with a flexible membrane. The ablation target was in the posterior part of the thalamic central lateral nucleus, a center associated with neuropathic pain. Details on the procedure and clinical results are described in Martin et al. (3).

Anonymized datasets from 5 patients were evaluated. The images were acquired with a spoiled gradient echo sequence using a custom designed 8-element phased array (similar to a cardiac array) coil wrapped around the transcranial FUS transducer (the coil is not shown in Fig. 1). Imaging parameters were TE/TR = 18.6/37.6 ms, BW = 7.36 kHz, FOV = 28 cm, slice thickness = 3 mm, flip angle = 30°, matrix size = 256×128, NEX = 1, acquisition time approximately 5 sec per image. Each dataset consisted of 9 to 11 images acquired consecutively over time during the thermal ablation, resulting in a total scan time of 40–55 seconds per sonication. The total number of sonications each patient received varied between 13 and 25 (mean 18.4). Sets were acquired predominantly in a sagittal orientation (total 62), followed by axial orientation (total 29), with only a few coronal datasets (total 2). For temperature reconstruction and statistical analysis, we used 8 datasets from each patient, 5 in a sagittal orientation and 3 in an axial orientation. The first image in each dataset was acquired before the onset of FUS delivery and was used as a baseline image. We reconstructed temperature images of each dataset using single baseline subtraction (SB) and hybrid reconstruction (hybrid SB+R). Since only a single image was acquired before each ablation we did not perform multi-baseline reconstructions. We visually compared temperature artifacts in the resulting temperature images, and generated temporal temperature uncertainty maps from the time series. For statistical analysis we selected three 3×3-pixel ROIs: in sagittal images the ROIs were located in the parietal region, the frontal region, and the cerebellum; in the axial images they were located in the temporal and occipital regions, as seen in Fig. 2.

Statistical Analysis

To compare the precision of the different methods, nonparametric tolerance intervals with 99% confidence and 99% coverage were calculated. For the patient data sets, the tolerance intervals were calculated for single baseline (SB) and hybrid with single baseline image in library (hybrid SB+R) by ROI and imaging plane; for the volunteer datasets, the tolerance intervals were calculated for single baseline (SB), multibaseline (MB), and hybrid with a single baseline (hybrid SB+R) and multibaseline library (hybrid MB+R). In addition, the percentage of measurements exceeding a criterion of ± 1°C temperature error was calculated for both methods, and the difference tested with a test of paired proportions (McNemar's test, with a Benferroni-adjusted critical p-value of 0.05/12 = 0.0042). For the test, single baseline (SB) was compared to hybrid with single baseline (hybrid SB+R), and multibaseline (MB) was compared to hybrid with a multibaseline library (hybrid MB+R). All statistical analyses were performed using Stata Release 11.1 (StataCorp LP, College Station, TX).

Results

Volunteer data

Results of the different temperature reconstruction methods of one volunteer are shown in Fig. 3, which shows the maximum temperature error over the first 5 temperature images

(upper row) and temporal temperature uncertainty over all 50 treatment images. Inspecting an image loop of the magnitude images over the approximately 4 minutes of imaging time of this particular volunteer showed minimal head motion (in-plane rotation around the atlantoaxial joint resulting in less than 1 mm motion at the front of the skull). In addition, brain pulsation inside the skull was visible with motion being most prominent in the front of the brain.

Figure 3 shows that single baseline subtraction (SB) results in considerable temperature errors across the brain with more than 6°C at the frontal cortex and the base of the skull, and 4°C or more in the center of the brain. Fluctuations over time are very visible. Averaging the baseline images (AB) resulted in little improvement in the absolute temperature error. Multibaseline subtraction (MB) considerably reduced the artifacts to 4°C in the front and less than 2°C in the center of the brain, with few pixels exceeding these values. Fluctuations are reduced but still present. When the hybrid method is used with a single baseline image (Hybrid SB+R), considerable improvements are visible across the brain compared to single and averaged baseline subtraction, however, errors still reach 6°C at the frontal cortex and the base of the skull, and up to 4°C near the ventricles. The hybrid method with a multibaseline library (Hybrid MB+R) achieved the lowest temperature errors. Maximum errors in the front, base and center of the brain are comparable to the multibaseline (MB) method with 4°C or less and 2°C, respectively, but fewer pixels are reaching these values. Fluctuations over time were much reduced and hardly noticeable. In all images and all reconstruction methods, ghosting from pulsatile flow was visible, particularly near the base of the skull.

Results of the statistical analysis in the three ROIs for all volunteers combined are summarized in Table 1. The results show that the hybrid reconstructions (both Hybrid SB+R and Hybrid MB+R) achieve substantially lower errors than single baseline (SB) and multibaseline subtraction (MB) alone. Errors with single baseline (SB) are highest with 48% of the pixels exceeding an error of 1°C. Errors with multibaseline (MB) are reduced, but even with 30 baseline images in the library, 36% of the pixels still have an error exceeding 1°C. If the hybrid method is used even with only a single baseline image (Hybrid SB+R), only 8% of the pixels exceed the 1°C threshold. For hybrid with a multibaseline library of 30 images (Hybrid MB+R), this is further reduced to just 2% of the pixels having an error of more than 1°C. Table 1 also lists the temperature errors for each of the ROIs individually. The differences between the number of pixels exceeding a 1°C temperature error with baseline subtraction and hybrid methods are significant at $P < 0.0001$ by McNemar test. To visualize the distribution of temperature errors, the temperature errors for each pixel in ROI #3 are plotted in Fig. 4. Both single baseline (SB) and multibaseline (MB) methods show substantial bias towards positive temperature errors. This bias is much reduced in both hybrid methods, especially in Hybrid MB+R, although a small bias remains.

Tongue and jaw movement as well as taking a deep breath, all caused noticeable temperature errors at the base of the skull in single baseline (SB) or multibaseline (MB) subtraction, whereas errors in hybrid imaging (Hybrid SB+R and Hybrid MB+R) were very small or not noticeable. In all tasks except tongue movement small head motion was visible while the volunteers performed the task. Figure 5 shows temperature images and temporal temperature uncertainty maps from a volunteer who was asked to perform tongue motion during the MR scan. The change in background phase caused by the tongue motion results in a temperature error in a large area at the base of the skull when using single baseline subtraction (SB). Hybrid reconstruction (Hybrid SB+R) is immune to this phase shift and accurately measures the temperature.

Patient data

Two typical magnitude images of the temperature imaging sequence in sagittal and axial scan planes are shown in Fig. 2. Bright water signal outside the head from the water-filled transducer is perturbed by the ultrasound, resulting in a heterogeneous appearance. Signal dropout and artifacts are seen in the frontal region of the brain in the axial image, which are caused by the presence of the stereotactic frame.

Temporal temperature uncertainty maps of two different sonications in axial and sagittal plane reconstructed with single baseline subtraction (SB) and the hybrid method (Hybrid SB +R) are shown in Fig. 6. The heating areas (black arrows) appear as regions of high uncertainty. Artifacts and signal dropout in the front of the brain near the stereotactic frame and flow artifacts from pulsating vessels (white arrow) also appear as high uncertainty. Overall, temperature uncertainty is substantially reduced in the hybrid method (Hybrid SB +R) compared to single baseline subtraction (SB) in all areas of the brain.

Results of the statistical analysis in the three ROIs in coronal and sagittal slices for all patients combined are summarized in Table 2. The results show that the hybrid reconstruction with a single baseline (Hybrid SB+R) achieves substantially lower errors than single baseline subtraction (SB) in all ROIs. With single baseline (SB), errors averaged over all ROIs are highest in sagittal images with 43% of the pixels and only slightly lower in axial images with 35% of the pixels exceeding an error of 1°C. Hybrid reconstruction (Hybrid SB+R) substantially reduces the errors to 5% of pixels in both sagittal and axial slices. The differences between the number of pixels exceeding a 1°C temperature error with baseline subtraction and hybrid methods are significant at $P < 0.0001$ by McNemar test.

A severe case of temperature errors during a FUS treatment is shown in Fig. 7. Magnitude images of the time series showed that brain motion was present and it appeared that the patient was moving his tongue or possibly speaking. The temperature images using single baseline subtraction (SB) show temperature errors across the brain with errors exceeding 3°C at the base of the skull and the cerebellum. Images reconstructed with the hybrid method (Hybrid SB+R) show a clear depiction of the heating spot, almost completely removing the errors present in baseline subtraction.

Discussion

Our results show that temperature reconstruction techniques developed for moving organs can be utilized to significantly decrease temperature errors during transcranial MR-guided focused ultrasound procedures. Several sources of motion were present in both patient and volunteer datasets, including bulk skull motion, brain and CSF pulsation, and jaw or tongue motion and swallowing. These kinds of motion caused substantial errors in the MR temperature images when baseline subtraction techniques are used for reconstruction.

The volunteer datasets showed that single baseline subtraction (SB) exhibited large temperature errors in the front of the skull, where pulsatile motion was most prominent. Averaging baseline images (AB) did not improve the errors; in individual time frames it even increased the error in some parts of the brain. This is not surprising since the averaged baseline includes images from various stages of the brain pulsation. Both, multibaseline (MB) and hybrid reconstruction with 30 library images (Hybrid MB+R) worked well in reducing errors. The multibaseline library contains images from various stages of brain and CSF pulsation, which allows removal of most errors due to this repetitive motion. Although the Hybrid MB+R shows little improvement compared to multibaseline (MB) processing in the datasets where volunteers had the instruction to remain as still as possible, the advantage of the hybrid method becomes clear in the datasets where non-repetitive motion is present.

In the datasets where the volunteers were instructed to perform tongue or jaw motion, to swallow or take a deep breath, multibaseline (MB) reconstruction was not able to correct for the resulting susceptibility changes and substantial temperature errors occurred. In the hybrid method (Hybrid MB+R), however, the referenceless component was able to suppress these artifacts resulting in reliable temperature estimation. We included in our volunteer analysis the hybrid method with a single baseline in the library (Hybrid SB+R), both for comparison with the patient data which only had a single baseline available and to see the influence of adding the referenceless component (+R) to the reconstruction. Errors were reduced across the brain compared to single (SB) and averaged baseline (AB) subtraction. However, large errors remained at the frontal cortex and near the ventricles. These are areas, where the background phase is not homogenous, but rather varies rapidly with the underlying anatomy. The referenceless (+R) component is designed to remove low spatially varying phase components which occur due to breathing, tongue motion, etc. but does not reduce high spatially varying phase components due to the anatomy.

The volunteer results also show that the baseline subtraction methods (SB and MB) have a large bias towards positive errors. These bias errors are typical for susceptibility induced background phase changes caused by breathing or tissue motion outside the imaging area. In the hybrid method, these phase changes are automatically corrected by the referenceless (+R) component. Looking at the percentage of pixels with an error > 1°C in Table 1 for the different methods shows that multibaseline (MB) has a much higher value as hybrid with a single baseline image (Hybrid SB+R). This seems to be contradict the results in Fig. 3, where multibaseline (MB) displays lower errors than Hybrid SB+R. This is due to the fact that the statistical analysis was done within the ROIs in Fig. 2, which are all located within the brain away from the cortex or base of the skull. These are areas where the background phase has small anatomical variations, benefitting the methods with just a single baseline (SB and Hybrid SB+R) because small motion due to pulsation or head movement will only cause minimal errors within the areas of homogenous background phase. We did not include ROIs at brain surface since focusing the ultrasound close to the skull is not feasible.

We did not include Referenceless reconstruction by itself into the analysis. The referenceless method is designed to estimate a background phase over a certain region in an organ. The region has to be large enough to include the heating region and provide sufficient area larger than the heating region to calculate a good background phase estimate, but it is not well suited to estimate the temperature across the whole brain. The assumption that the background phase can be represented by a low order polynomial across the whole brain is not valid, especially in the frontal region and the base of the brain, which is close to air filled sinuses and nasal cavities with large susceptibility differences. While the phase differences outside the heated region are low spatial frequency, the background phase in each image is not. Since whole brain coverage is important for transcranial MRgFUS application to visualize potential heating in the near and far-field of the ultrasound beam near the skull, we did not further investigate referenceless reconstruction by itself in this work.

In the patient datasets we only compared two reconstruction methods: single baseline subtraction (SB) and hybrid reconstruction with a library size of one (Hybrid SB+R). It was not possible to investigate multibaseline (MB) subtraction or Hybrid MB+R, since only a single baseline image was acquired before the onset of the focused ultrasound ablation. However, even with a single baseline image in the library, the hybrid algorithm substantially reduces the temperature error compared to baseline subtraction. Since the patients are awake during the transcranial MRgFUS procedure, it is very likely that events such as tongue motion, swallowing or deep breathing occur, which result in severe artifacts with baseline subtraction as seen in Fig. 7. These problems are not an issue with the hybrid method

(Hybrid SB+R), as the referenceless (+R) component of the algorithm removes any artifacts created by a smooth phase changes due to these events.

Cerebral spinal fluid (CSF) and brain motion are associated since brain pulsation is the driving force for CSF motion. Both, brain motion and CSF motion, can be a cause for temperature errors: brain motion changes the phase due to tissue displacement, whereas CSF motion changes the phase due to variable velocity of the moving fluid. However, both these phase or temperature errors are reduced when a multibaseline method (MB and Hybrid MB +R) is used, because the multibaseline library contains images from various stages of brain and CSF pulsation. This can be appreciated in Fig. 3, where errors from CSF in the ventricles are much smaller in the multibaseline methods (MB and Hybrid MB+R) compared to the single baseline methods.

The volunteer and patient data sets were acquired with different imaging parameters. The patient images were retrospectively reconstructed from datasets acquired during transcranial MRgFUS procedures (3). For the volunteer data sets, we used a protocol with shorter TE and TR values than in the patient data sets. Our volunteer protocol is based on InSightec's new protocol for transcranial MRgFUS for the currently ongoing tremor trials (4). We used the imaging parameters in the protocol without attempting to optimize the values for the volunteer study as conditions for the transcranial MRgFUS procedures are very different with the FUS transducer, electronics, stereotactic frame, and water bath present. An optimization should therefore be performed with the actual setup, which was beyond the scope of this comparison of reconstruction methods.

In this work, temperature images reconstructed with baseline subtraction (SB and MB) were not compensated for phase drift. Phase drift is caused by a temporal instability of the magnetic flux and can be measured and potentially corrected with a reference phantom that remains at a fixed temperature (21) or by choosing an ROI in a non-heated area. In our datasets, we did not see a spatially constant drift that could be compensated with a single drift correction ROI. Rather, regions close to the drift correction ROI might improve, but areas further away showed an increase in temperature error compared to no drift correction. Figures 5 and 7 are examples where a drift ROI in an inappropriate location can increase temperature errors. Since results varied depending on the location of the correction ROI, and since it was difficult to determine an ROI that would improve and not worsen the overall result, we did not perform a drift correction. The hybrid method does not require a drift correction as the referenceless (+R) component automatically corrects for any phase drifts.

It is not clear from this study what baseline library size would be most useful for this application. Ideally, the library should be large enough to sample different pulsation stages, but small enough to avoid redundant library images, which would cost additional acquisition time. If accurate temperatures are only desired inside the brain, away from the cortex, Hybrid SB+R is working well. If accurate temperature measurements are need at the cortex, e.g. to visualize heating from the skull, Hybrid MB+R is better, but will cost additional time. Experiments to determine the optimal number of baseline images required have been presented elsewhere (22).

In summary, our results show that the hybrid method for temperature reconstruction is beneficial to monitor FUS ablation in the brain. Using the hybrid method with a library of baseline images (Hybrid MB+R) achieves the best results. But even with a single baseline image in the library (Hybrid SB+R), the hybrid method substantially reduces temperature errors. The pure baseline subtraction methods (SB and MB) are not able to correct for non-repetitive motion. By adding the referenceless (+R) component, the hybrid algorithm

becomes robust to spontaneous events such as swallowing, jaw or tongue movement, or changes in respiration.

Acknowledgments

We would like to thank Dr. Nathan McDannold from Brigham and Women's Hospital for helpful discussions and acknowledge our grant support, NIH R00 HL097030, NIH R21 EB011559, NIH P41 RR009784, and NIH P01 CA159992.

Grant Sponsor: NIH (R00 HL097030, R21 EB011559, P41 RR009784, and P01 CA159992)

References

1. Jolesz FA, Hynynen K, McDannold N, Tempany C. MR Imaging–Controlled Focused Ultrasound Ablation: A Noninvasive Image-Guided Surgery. Magnetic Resonance Imaging Clinics of North America. 2005 Aug; 13(3):545–560. [PubMed: 16084419]
2. McDannold N, Clement GT, Black P, Jolesz F, Hynynen K. Transcranial Magnetic Resonance Imaging– Guided Focused Ultrasound Surgery of Brain Tumors. Neurosurgery. 2010 Feb; 66(2): 323–332. [PubMed: 20087132]
3. Martin E, Jeanmonod D, Morel A, Zadicario E, Werner B. High-intensity focused ultrasound for noninvasive functional neurosurgery. Ann Neurol. 2009 Dec; 66(6):858–861. [PubMed: 20033983]
4. Elias, J.; Huss, D.; Loomba, J.; Khaled, M.; Frysinger, R.; Sperling, S., et al. A phase 1 study of MR-guided focused ultrasound thalamotomy for the treatment of medication-refractory essential tremor; Focused Ultrasound 2012, 3rd International Symposium; 2012.
5. Colen, RR.; Jolesz, F. Neuroimaging Clinics of NA. Vol. 20. Elsevier Ltd; 2010 Aug 1. Future Potential of MRI-Guided Focused Ultrasound Brain Surgery; p. 355-366.
6. Leonardi MA, Lumenta CB, Gumprecht HK, Einsiedel von GH, Wilhelm T. Stereotactic guided laser-induced interstitial thermotherapy (SLITT) in gliomas with intraoperative morphologic monitoring in an open MR-unit. Minim Invasive Neurosurg. 2001 Mar; 44(1):37–42. [PubMed: 11409310]
7. Ishihara Y, Calderon A, Watanabe H, Okamoto K, Suzuki Y, Kuroda K, et al. A precise and fast temperature mapping using water proton chemical shift. Magn Reson Med. 1995 Dec; 34(6):814–823. [PubMed: 8598808]
8. Rieke V, Butts-Pauly K. MR thermometry. J Magn Reson Imaging. 2008 Feb; 27(2):376–390. [PubMed: 18219673]
9. Vigen KK, Daniel BL, Pauly JM, Butts K. Triggered, navigated, multi-baseline method for proton resonance frequency temperature mapping with respiratory motion. Magn Reson Med. 2003 Oct 24; 50(5):1003–1010. [PubMed: 14587011]
10. de Senneville BD, Mougenot C, Moonen CTW. Real-time adaptive methods for treatment of mobile organs by MRI-controlled high-intensity focused ultrasound. Magn Reson Med. 2007; 57(2):319–330. [PubMed: 17260361]
11. Rieke V, Vigen KK, Sommer G, Daniel BL, Pauly JM, Butts K. Referenceless PRF shift thermometry. Magn Reson Med. 2004 Jun; 51(6):1223–1231. [PubMed: 15170843]
12. Kuroda K, Kokuryo D, Kumamoto E, Suzuki K, Matsuoka Y, Keserci B. Optimization of self-reference thermometry using complex field estimation. Magn Reson Med. 2006; 56(4):835–843. [PubMed: 16944467]
13. Grissom WA, Lustig M, Holbrook AB, Rieke V, Pauly JM, Butts-Pauly K. Reweighted $\ell 1$ referenceless PRF shift thermometry. Magn Reson Med. 2010 Oct; 64(4):1068–1077. [PubMed: 20564600]
14. Grissom WA, Rieke V, Holbrook AB, Medan Y, Lustig M, Santos J, et al. Hybrid referenceless and multibaseline subtraction MR thermometry for monitoring thermal therapies in moving organs. Med Phys. 2010 Sep; 37(9):5014–5026. [PubMed: 20964221]
15. Greitz D, Wirestam R, Franck A, Nordell B, Thomsen C, Ståhlberg F. Pulsatile brain movement and associated hydrodynamics studied by magnetic resonance phase imaging. The Monro-Kellie doctrine revisited. Neuroradiology. 1992; 34(5):370–380. [PubMed: 1407513]

16. Enzmann DR, Pelc NJ. Brain motion: measurement with phase-contrast MR imaging. Radiology. 1992 Dec; 185(3):653–660. [PubMed: 1438741]

17. Peters NHGM, Bartels LW, Sprinkhuizen SM, Vincken KL, Bakker CJG. Do respiration and cardiac motion induce magnetic field fluctuations in the breast and are there implications for MR thermometry? J Magn Reson Imaging. 2009 Feb 25; 29(3):731–735. [PubMed: 19243069]

18. Kickhefel, A.; Roland, J.; Weiss, C.; Schick, F. Physica Medica. Vol. 26. Elsevier Ltd; 2010 Jan 20. Accuracy of real-time MR temperature mapping in the brain: A comparison of fast sequences; p. 192-201.

19. Shmatukha AV, Bakker CJG. Correction of proton resonance frequency shift temperature maps for magnetic field disturbances caused by breathing. Phys Med Biol. 2006 Sep 4; 51(18):4689–4705. [PubMed: 16953050]

20. Vigen KK, Jarrard J, Rieke V, Frisoli J, Daniel BL, Butts-Pauly K. In vivo porcine liver radiofrequency ablation with simultaneous MR temperature imaging. J Magn Reson Imaging. 2006 Apr; 23(4):578–584. [PubMed: 16508928]

21. De Poorter J. The Proton-Resonance-Frequency-Shift Method Compared with Molecular Diffusion for Quantitative Measurement of Two-Dimensional Time-Dependent Temperature Distribution in a Phantom. J Magn Reson B. 1994 Mar; 103(3):234–241.

22. Instrella, R.; Butts Pauly, K.; Grissom, W.; Rieke, V. Reduction of motion artifacts in MRgFUS in the brain using hybrid thermometry; Proceedings of the 20th Annual Meeting of ISMRM; Melbourne, Australia. 2012.

Figure 1.
Patient setup for transcranial MR-guided focused ultrasound intervention. The head is immobilized within a stereotactic frame. The flexible membrane seals the space between patient head and transducer, which is filled with degassed water.

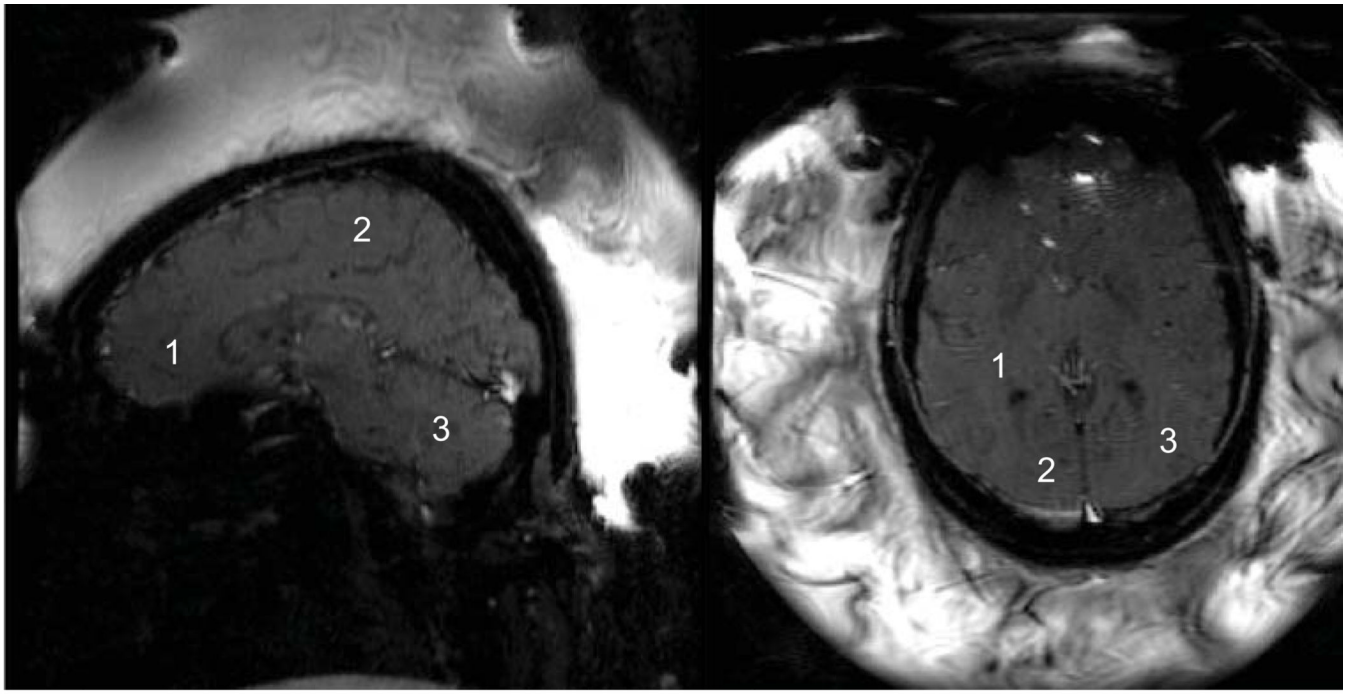

Figure 2.
Typical sagittal and axial magnitude images of the temperature sensitive gradient echo sequence used during sonication. Bright water signal outside the head from the water-filled transducer is perturbed by the ultrasound, resulting in a heterogeneous appearance. The sagittal image shows the position of the ROIs in the frontal, parietal, and cerebellum regions used for analysis. The axial slice shows signal dropout in the frontal region of the brain caused by the proximity of the stereotactic frame. ROIs are located in the temporal and occipital regions.

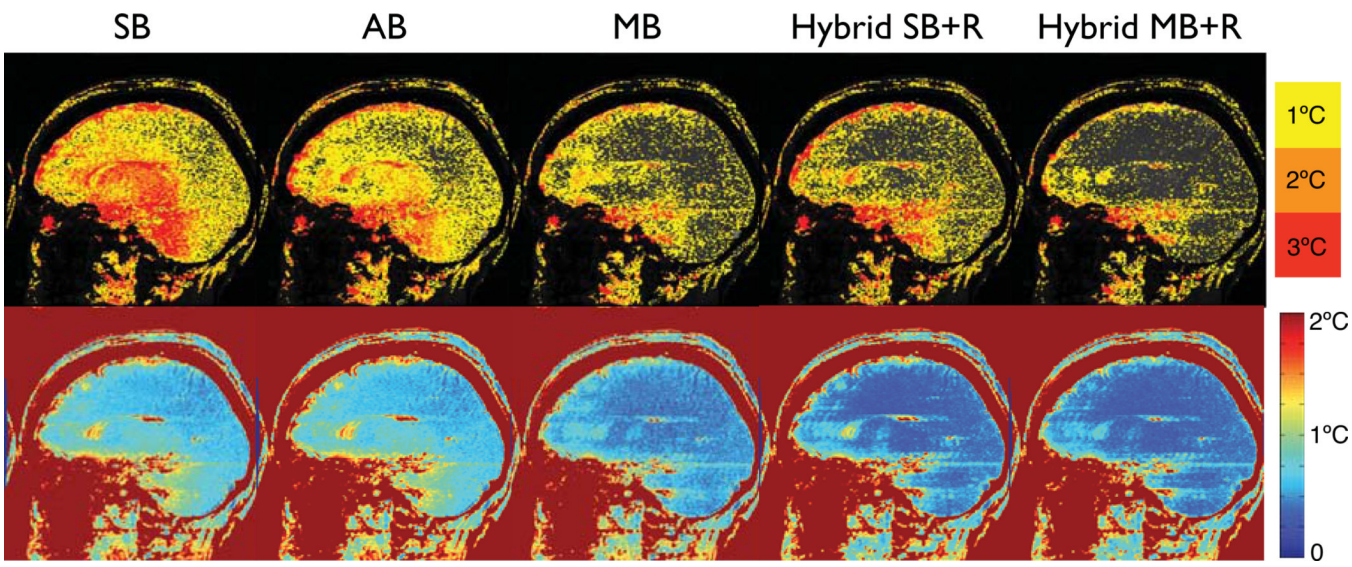

Figure 3.
Upper row: Maximum absolute error of the different temperature reconstruction methods over the first 5 images in a volunteer without heating. Lower row: Temporal temperature uncertainty over all 50 treatment images in the dataset. Single baseline subtraction (SB) results in substantial errors across the brain. Averaging the baseline images (AB) achieves only minor improvements. Multi-baseline (MB) reduces the errors considerably. Hybrid with a single baseline image (Hybrid SB+R) achieves lower errors than single or averaged baseline subtraction, but errors are still high, particularly a the frontal cortex and base of the skull. Hybrid reconstruction with a multi-baseline library (Hybrid MB+R) achieves the best results of all methods.

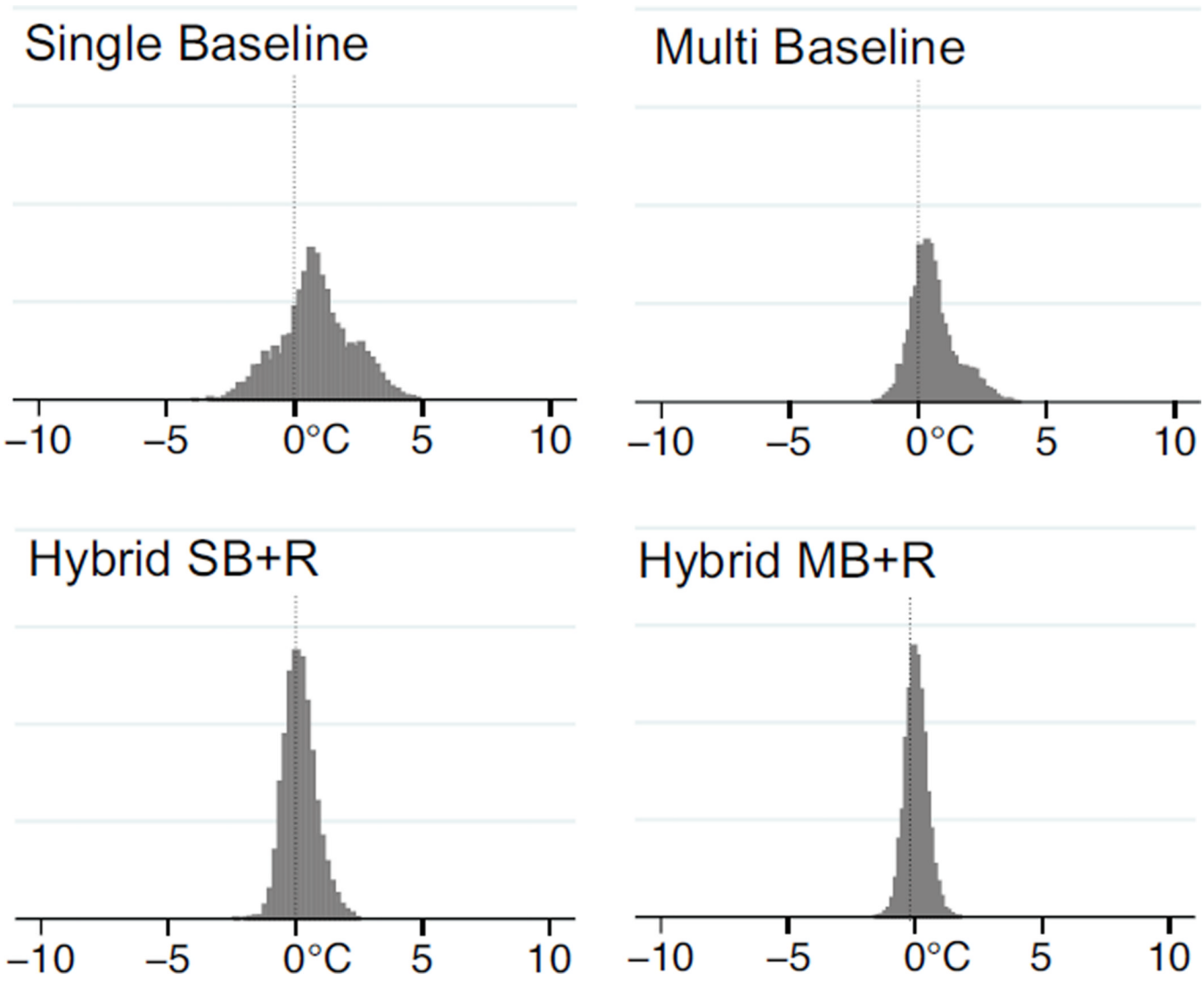

Figure 4.
Distribution of temperature error of the different methods for a single ROI (ROI #3) in all volunteer datasets.

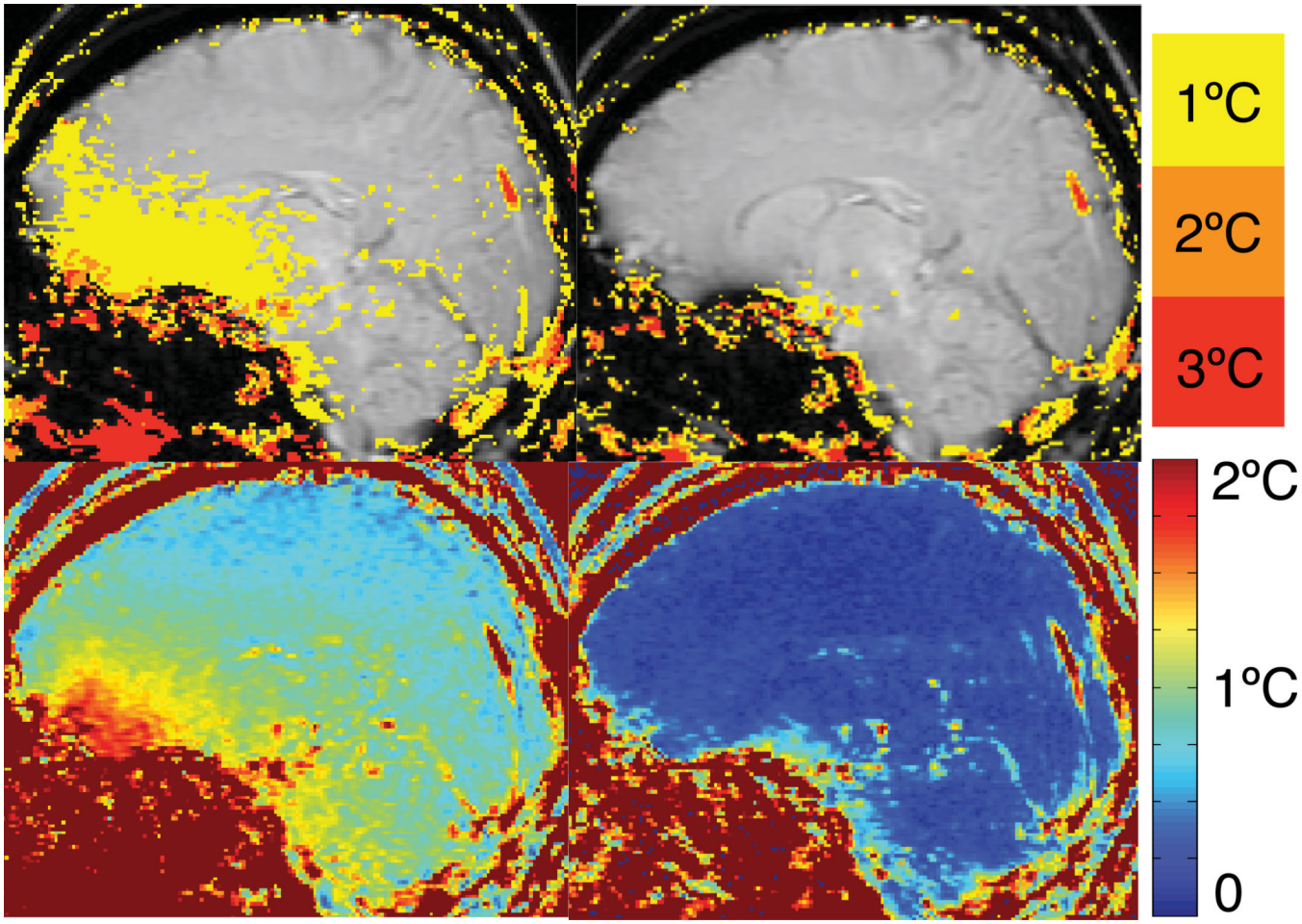

Figure 5.
Temperature images (top row) and temporal temperature uncertainty maps (bottom row) from a volunteer who was asked to perform tongue motion during the scan. The change in background phase caused by the tongue motion results in a temperature error in a large area at the base of the skull when using single baseline subtraction (SB). Hybrid reconstruction (Hybrid SB+R) is immune to this phase shift and accurately measures the temperature.

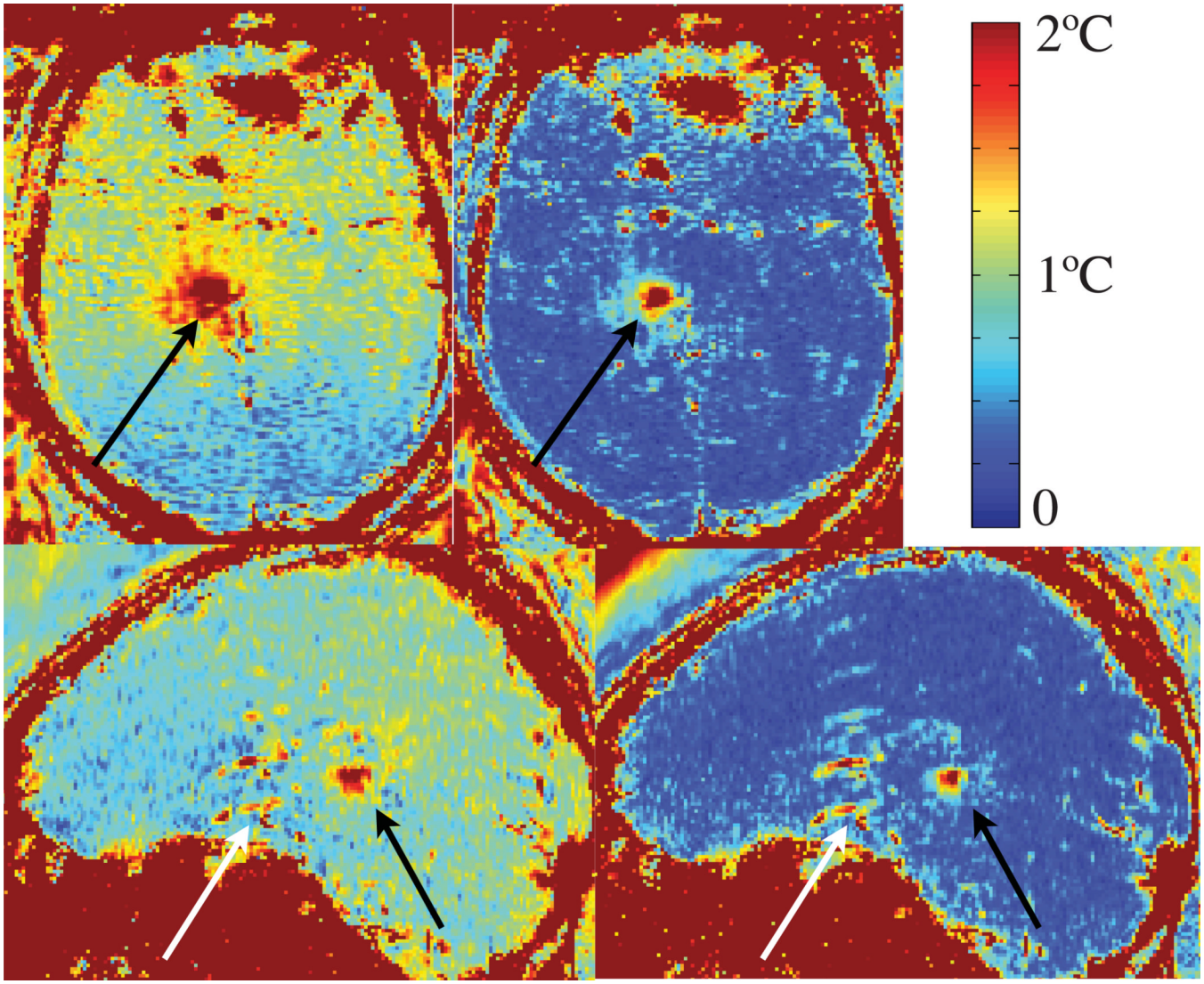

Figure 6.

Temporal temperature uncertainty maps of two different sonications in axial and sagittal plane reconstructed with baseline subtraction and hybrid method. The heating areas (black arrows) appear as high uncertainty. Artifacts and signal dropout in the front of the brains from the stereotactic frame and flow artifacts from pulsating vessels (white arrows) also appear as high uncertainty. Overall, temperature uncertainty is substantially reduced in the hybrid method (Hybrid SB+R) compared to single baseline subtraction (SB) in all areas of the brain.

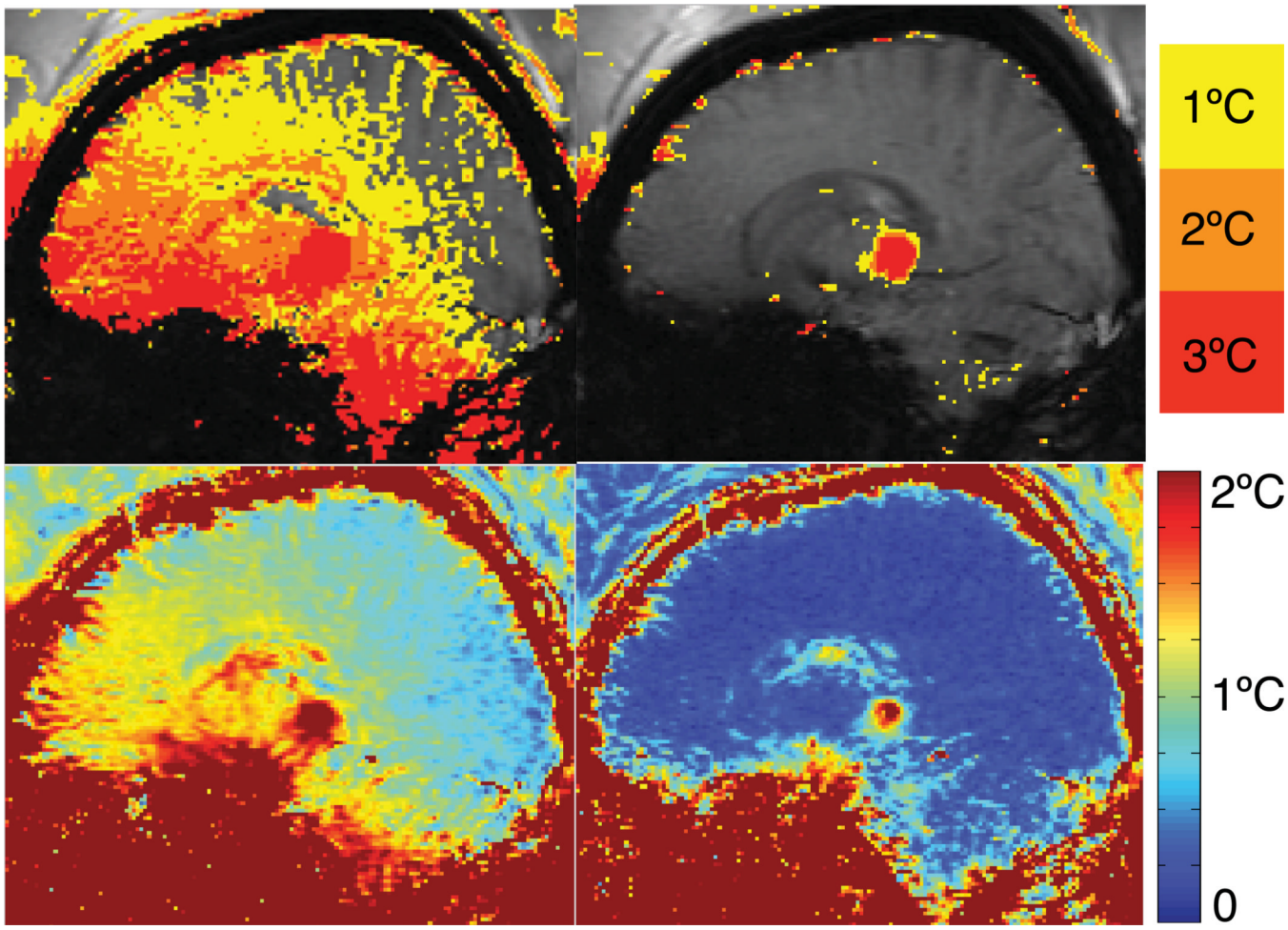

Figure 7.
Temperature maps (upper row) and temporal temperature uncertainty (bottom row) of a patient undergoing FUS ablation. Single baseline subtraction (SB) shows severe errors due to brain motion. Hybrid reconstruction (Hybrid SB+R) shows a clear depiction of the heating spot, almost completely removing the severe errors present with single baseline subtraction (SB).

Table 1

Results of volunteer datasets for three ROI in sagittal plane.

Method	ROI	99% Tolerance Interval	pixel with error > 1°C
Single baseline	1	−2.7°C – 4.5°C	54%
	2	−1.7°C – 3.1°C	36%
	3	−2.6°C – 4.3°C	52%
	All	−2.4°C – 4.0°C	48%
Multi baseline	1	−1.4°C – 3.8°C	50%
	2	−1.0°C – 2.6°C	32%
	3	−1.6°C – 2.8°C	27%
	All	−1.5°C – 3.2°C	36%
Hybrid SB/R	1	−1.4°C – 1.5°C	8%
	2	−1.4°C – 1.1°C	6%
	3	−1.3°C – 1.7°C	11%
	All	−1.4°C – 1.5°C	8%
Hybrid MB/R	1	−0.9°C – 1.2°C	4%
	2	−0.9°C – 0.8°C	1%
	3	−1.0°C – 1.1°C	2%
	All	−1.0°C – 1.1°C	2%

The 99% tolerance interval indicates the limits within which 99% of future observations with each method should fall with 99% confidence. Differences between hybrid and non-hybrid number of pixels exceeding a 1°C temperature error are significant at $P < 0.0001$ by McNemar test.

Table 2

Results of patient data sets for three ROIs in axial and sagittal plane.

Plane	Method	ROI	99% Tolerance Interval	pixel with error > 1°C
Axial	Single baseline	1	−3.1°C – 2.2°C	37%
		2	−3.1°C – 2.6°C	37%
		3	−3.0°C – 2.0°C	31%
		All	−3.1°C – 2.3°C	35%
	Hybrid SB/R	1	−1.2°C – 1.3°C	5%
		2	−1.3°C – 1.3°C	6%
		3	−1.2°C – 1.2°C	5%
		All	−1.2°C – 1.3°C	5%
Sagittal	Single baseline	1	−5.2°C – 7.1°C	43%
		2	−3.0°C – 3.1°C	38%
		3	−3.9°C – 4.1°C	48%
		All	−4.4°C – 5.1°C	43%
	Hybrid SB/R	1	−1.3°C – 1.3°C	6%
		2	−1.1°C – 0.9°C	2%
		3	−1.4°C – 1.3°C	6%
		All	−1.3°C – 1.2°C	5%

The 99% tolerance interval indicates the limits within which 99% of future observations with each method should fall with 99% confidence. Differences between hybrid and non-hybrid number of pixels exceeding a 1°C temperature error are significant at $P < 0.0001$ by McNemar test.